NANO LETTERS

Letter

pubs.acs.org/NanoLett

Quantum Yield of Single Surface Plasmons Generated by a Quantum Dot Coupled with a Silver Nanowire

Qiang Li,[†] Hong Wei,*[,†] and Hongxing Xu[†,‡]

[†]Beijing National Laboratory for Condensed Matter Physics, Institute of Physics, Chinese Academy of Sciences, Beijing 100190, China

[‡]Center for Nanoscience and Nanotechnology, School of Physics and Technology, and Institute for Advanced Studies, Wuhan University, Wuhan 430072, China

Supporting Information

ABSTRACT: The interactions between surface plasmons (SPs) in metal nanostructures and excitons in quantum emitters (QEs) lead to many interesting phenomena and potential applications that are strongly dependent on the quantum yield of SPs. The difficulty in distinguishing all the possible exciton recombination channels hinders the experimental determination of SP quantum yield. Here, we experimentally measured for the first time the quantum yield of single SPs generated by the exciton−plasmon coupling in a system composed of a single quantum dot and a silver nanowire (NW). By utilizing the SP guiding property of the NW, the decay rates of all the exciton recombination channels, i.e., direct free space radiation channel, SP generation channel, and nonradiative damping channel, are quantitatively obtained. It is determined that the optimum emitter-NW coupling distance for the largest SP quantum yield is about 10 nm, resulting from the different distance-dependent decay rates of the three channels. These results are important for manipulating the coupling between plasmonic nanostructures and QEs and developing on-chip quantum plasmonic devices for potential nanophotonic and quantum information applications.

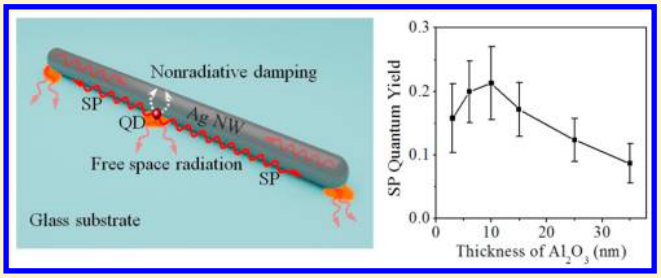

KEYWORDS: *Quantum dot, silver nanowire, exciton, surface plasmons, quantum yield, decay rates*

The interactions between surface plasmons (SPs) and excitons in the coupled systems composed of metal nanostructures and quantum emitters (QEs) are of considerable current interest.[1−4] Mediated by SPs that are the collective oscillations of free electrons on the metal surface driven by electromagnetic waves,[5,6] the coupled systems show many interesting phenomena and enable many potential applications, such as plasmon-enhanced fluorescence,[7−10] plasmon-mediated energy transfer,[11,12] plasmon-enhanced light-emitting diodes,[13] exciton−plasmon−photon conversion,[14,15] and plasmonic amplifier and nanolaser.[16−18] All of these phenomena and device applications are strongly dependent on the efficiency of excitons converting to SPs, i.e., the quantum yield of SPs. As is known, there are three channels for the recombination of the excitons in coupled plasmonic systems, which are the direct free space radiation channel, SP generation channel, and nonradiative damping channel. To get the SP quantum yield, the decay rates of all these three channels need be determined. To separate the nonradiative damping from the exciton recombination processes, there are only two reported methods as far as we know. One is to utilize the nearly uninfluenced excitation rate when the excitation wavelength is far from the SP resonance.[19] The other one is based on the assumption that the enhancement factor of excitation rate is the same as that of the radiative decay rate when the excitation wavelength is close enough to the emission wavelength of QEs.[20] However, there is still no experimental method that can separate the SP generation channel with the direct free space radiation channel. The experimentally measured emission intensity and radiative decay rates are usually convoluted values of the direct radiation from the emitters and the scattering of exciton-generated SPs,[21−23] because the photons emitted through these two channels are indistinguishable. This indistinguishability hinders the determination of SP quantum yield.

The propagating SPs supported by the metal nanowire (NW) make it possible to separate the directly emitted photons and the generated SPs in the QE-NW coupling structure, which provides a suitable system to disentangle the exciton recombination channels and obtain the SP quantum yield.[24,25] In recent years, the coupling between QEs and metal NWs has received strong interest.[1,14,15,24−35] The tight confinement of the optical field associated with the guided SPs along the NW enables the strong interaction with individual QEs. In particular, the exciton−plasmon coupling has been achieved with single quantum dot (QD)[24,25,31] and NV-

Received: September 10, 2015
Revised: November 13, 2015
Published: November 19, 2015

DOI: 10.1021/acs.nanolett.5b03654
Nano Lett. 2015, 15, 8181−8187

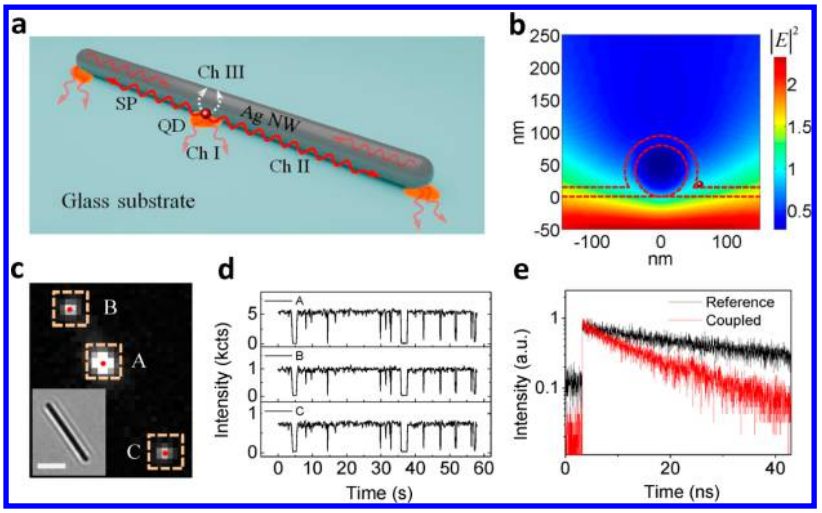

Figure 1. Coupling of single QD to Ag NW. (a) The scheme for the exciton−plasmon coupling processes in the QD-NW system. The exciton in an excited QD can recombine through three channels: directly emitting photon to free space (Ch I, red arrows from the QD to the glass substrate), generating guided SP on the NW (Ch II, red wavy lines along the NW), and nonradiative damping (Ch III, white dotted arrows). The guided SP propagates along the NW with an energy attenuation process caused by the metal absorption. The SP is not only converted into photons at the NW ends but also reflected and then interferes with itself so that the NW acts as a Fabry−Pèrot resonator (see Supporting Information Figure S1). (b) Electric-field intensity $|E|^2$ distribution at the cross section of a glass-supported NW of 80 nm diameter coated with 15 nm Al_2O_3 when illuminated by a 532 nm wavelength Gaussian beam with polarization parallel to the NW axis. The intensity distribution is normalized by the intensity across the section without NW. The red dotted lines show the outlines of the Ag NW and the Al_2O_3 film. (c) PL image of a single QD coupled with a Ag NW coated with Al_2O_3 film of 15 nm thickness. The inset is the optical transmission image of the Ag NW. The scale bar is 2 μm. The red dots are the accurate positions of QD A and the NW ends obtained using single molecule localization method. (d) Time traces of fluorescence counts of QD A and scattered light at the NW ends B and C. The intensity unit kcts means 1000 counts. The light pink boxes in (c) show the regions where the counts of each pixel are integrated to generate the emission counts. (e) PL decay curves of an uncoupled reference QD (black line) and the coupled QD A (red line).

center,[28,29,33] resulting in the Purcell enhancement of QE spontaneous emission and the efficient generation of single SPs. The generation of single plasmons bridges the fields of nanoplasmonics and quantum optics and opens the prospects of using quantum optical techniques to study single plasmons and designing novel quantum plasmonic devices. Owing to the nanometer size, QDs are ideal QEs for local probing and excitation of plasmonic nanostructures with high spatial accuracy.[34,35] In the previous studies on the efficiency of QD emission into SPs,[24,25] the reported efficiency values are the results neglecting the nonradiative damping channel, a dominating decay channel for small QD-NW separation.[36] Therefore, they cannot reflect the real SP quantum yield. The experimental measurement of single SP quantum yield is thus highly desired.

In this work, we carefully analyzed the exciton−plasmon coupling process in a coupled system composed of a single QD and a silver NW. The quantum yield of single SP generation is determined for the first time by disentangling all the exciton recombination channels. Moreover, we used Al_2O_3 thin film with different thickness to control the QD-NW separation and studied the distance dependent exciton recombination dynamics. Our results show that the decay rates of exciton to all the three decay channels increase by decreasing QD-NW separation distance but with different increasing rates, which results in an optimum QD-NW distance of about 10 nm, corresponding to a maximum SP quantum yield of 21%.

In general, fluorescence from a QD under weak excitation (not saturated) is a two-step process, involving the excitation and subsequent fluorescent emission. The photoluminescence (PL) emission intensity of a QD on substrate can be described by $I_0 = C_0\gamma_{exc,0}\eta_{rad,0}$, where C_0 is the overall collection efficiency of the setup, $\gamma_{exc,0}$ is the excitation rate, $\eta_{rad,0}$ is the radiation quantum yield given by $\eta_{rad,0} = k_{rad,0}/(k_{rad,0} + k_{nrad,0}) = k_{rad,0}/k_{tot,0}$, where $k_{rad,0}$ and $k_{nrad,0}$ are the radiative and nonradiative decay rate, respectively. The excitation rate $\gamma_{exc,0}$ and radiative decay rate $k_{rad,0}$ are both proportional to the local density of optical states (LDOS),[37,38] while the nonradiative recombination is an intrinsic process of QD under the weak excitation condition.[39] If the QD on substrate is present in the vicinity of a silver NW, the exciton−plasmon coupling makes the QD relaxation process more complex. As schematically shown in Figure 1a, the excited QD nearby the NW can undergo energy relaxation through three possible channels:[24] radiative emission into free space (channel I), excitation of propagating single SP on the NW followed by scattering at two NW ends (channel II), and nonradiative damping (channel III) including both the intrinsic nonradiative decay of the QD and the metal-induced nonradiative damping. The last channel is of particular importance when the emitter is very close to the metal surface, as the metal-induced nonradiative damping will be significantly increased.[7,36] In analogy to the definition of quantum yield of radiation emission for emitters, we define the quantum yield of generating single SP for the QD coupled to a silver NW as

$$\eta_{SP} = \frac{k_{SP}}{k_{rad,m} + k_{SP} + k_{nrad,m}} \quad (1)$$

where $k_{rad,m}$ is the radiative decay rate, k_{SP} is the decay rate to SP generation channel, $k_{nrad,m}$ is the decay rate to nonradiative damping channel, and subscript m refers to the emitter coupled with metal nanostructure. The SP quantum yield η_{SP} indicates the ability of the NW to capture the energy of an emitter into the guided plasmon modes, which is important for characterizing the QD-NW coupling strength.

DOI: 10.1021/acs.nanolett.5b03654
Nano Lett. 2015, 15, 8181−8187

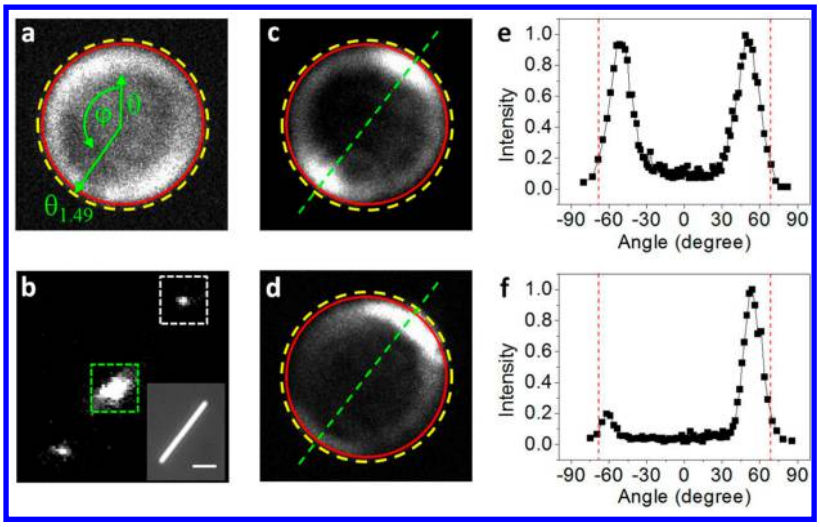

Figure 2. Angular distributions of emission from the QDs and the NW end scattering. (a) Fourier image of a single reference QD on glass substrate. The outer yellow dashed circle and inner red circle outline the maximum collection angle of the objective with NA = 1.49 and 1.4, respectively. The excitation polarization is in the direction of $\varphi = 90°$. (b) PL image showing the coupling of a single QD to a Ag NW coated with Al_2O_3 film of 10 nm thickness. The larger emission spot is the result of direct far-field emission from the QD near the NW, while two smaller spots correspond to the scattered SPs at the NW ends generated by the coupled QD. The inset is bright-field optical image of the NW. The scale bar is 2 μm. (c, d) Fourier images obtained from the areas marked by the green and white dashed squares in (b), corresponding to the radiation from the coupled QD (c) and the NW end scattering (d), respectively. The green dashed lines indicate the direction of the NW. (e, f) Emission intensity distribution versus θ along the green dashed lines in (c) and (d). The vertical lines correspond to the maximum radial collection angle of the objective with NA = 1.4.

For a QD in the vicinity of a Ag NW, both the excitation rate $\gamma_{exc,m}$ and total decay rate $k_{tot,m}(k_{tot,m} = k_{rad,m} + k_{SP} + k_{nrad,m})$ can be modified due to the changes of LDOS. The measured emission intensity ratio of the NW-coupled QD to the reference QD on substrate is written as

$$\frac{I_m}{I_0} = \frac{C_m}{C_0}\frac{\gamma_{exc,m}}{\gamma_{exc,0}}\frac{k_{rad,m}}{k_{rad,0}}\frac{k_{tot,0}}{k_{tot,m}} \quad (2)$$

The excitation rate is proportional to the local electric-field intensity at the position of QD, and the excitation rate enhancement factor can be expressed as the ratio of the local electric-field intensity with and without the NW. The simulation result in Figure 1b shows that the QD near the NW feels almost no change of excitation rate when the focused laser beam is polarized parallel to the NW (see Supporting Information Figure S2 for other thicknesses of Al_2O_3 film). Considering $k_{tot} = 1/\tau$ (τ is the PL lifetime), eq 2 can be rewritten as

$$k_{rad,m} \approx \frac{C_0}{C_m}\frac{I_m}{I_0}\frac{1}{\tau_m}\eta_{rad,0} \quad (3)$$

This expression shows that the radiative decay rate of the coupled QD can be obtained by measuring its PL intensity I_m and lifetime τ_m, if the PL intensity I_0 and radiation quantum yield $\eta_{rad,0}$ of the reference QD and the collection efficiency ratio C_0/C_m can be determined.

In our experiments, Ag NWs (about 80 nm in diameter) deposited on a glass substrate were coated with Al_2O_3 film of different thickness. Then CdSe/ZnS QDs with emission wavelength centered at about 650 nm were spin-coated onto the sample surface. The QDs were illuminated by 532 nm laser light polarized parallel to the NW axis through an oil immersion objective with NA = 1.4. The emitted fluorescence can be guided to an EMCCD for imaging or to single photon avalanche diodes for analysis using a time-correlated single photon counting module (see Section 3 of Supporting Information). The excitation power is 1 μW, which ensures that the excited QDs are well below the saturation condition (see Supporting Information Figure S3). Figure 1c shows the PL image of a single QD coupled with a Ag NW coated with 15 nm Al_2O_3 film. The bright spots A, B, and C correspond to the QD fluorescence and scattering of SPs at the NW ends, respectively. As shown in Figure 1d, the three time traces of PL counts from A, B, and C show the same ON/OFF blinking behavior, indicating that there is only one QD at spot A and the QD is the source of the single plasmons propagating along the NW (see Supporting Information Figure S4).

Figure 1e shows the fluorescence decay curves for QD A and an uncoupled reference QD on Al_2O_3-coated glass substrate. A single exponential decay fitting yields the PL lifetime of 11.6 and 28.6 ns for these two QDs, respectively. This reduction in lifetime of the coupled QD is mainly due to the increased LDOS near the NW, which is consistent with previous reports about the QDs coupled to plasmonic NWs.[24,25,30,33] We also compared the PL emission intensity of the QD A to that of the reference QDs on substrate (averaged intensity of 70 reference QDs) under the same excitation conditions. The result shows that the intensity ratio of the QD A to reference QDs is 0.86 ± 0.06. It is worth mentioning that the PL intensities of reference QDs are independent of the excitation polarization (see Supporting Information Figure S5), which is due to the spherically degenerated excitation transition dipole of single CdSe/ZnS QDs.[40]

It is known that the metal nanostructures can alter the angular distribution of emission from adjacent single QE.[41] This effect is especially pronounced for elongated NWs that can serve as optical antennas, which can drastically change the angular emission pattern and hence the fraction of light collected by the microscope objective.[42,43] In order to determine the collection efficiency of our setup, the angular intensity distribution of the emission from the reference QD, coupled QD, and wire end scattering was monitored on the

DOI: 10.1021/acs.nanolett.5b03654
Nano Lett. 2015, 15, 8181−8187

Fourier plane of an oil immersion objective with NA = 1.49. Here we moved a small aperture installed in the image plane of the microscope to ensure that only the photons from the interested area were detected. Figure 2a shows the obtained Fourier image of the radiation from a reference QD. The radial coordinate θ on the Fourier image scales as the numerical aperture NA = n sin θ, where n = 1.5 is the refractive index of the glass substrate. The outer yellow dashed circle and the inner red circle outline the maximum collection angle of the objectives with NA = 1.49 and 1.4, respectively. Because individual QD can be considered as a complex emitter with three orthogonal emission dipoles,[44,45] the radiation pattern of the reference QD is nearly isotropic in the azimuthal angle φ, which means that the emission of single QD can be expressed as a superposition of three orthogonal linear dipole emitters with similar emission intensity (see Section 7 of Supporting Information). Clearly, most of the emission light from reference QD radiated into glass substrate has been collected by the objective with NA = 1.4. The Fourier images of the radiation from a coupled QD (green dashed square in Figure 2b) and of the emitted light from the NW end (white dashed square in Figure 2b) are shown in Figure 2c,d, respectively. The direct far-field emission of the coupled QD shows a nearly symmetric pattern with respect to the NW axis (indicated by the green dashed line) with two bright lobes at the rims of the pattern (Figure 2c), which can be understood in terms of the interaction of the QD emission dipole with their induced image dipole in the Ag NW.[35] For the Fourier plane image of the scattering at the NW end (Figure 2d), the intensity distribution is in an arc shape with larger intensity along the NW direction, which means that the NW end emission is highly unidirectional.[46] The high directionality of the emission shown in Figure 2c,d indicates that the QD-NW coupled system can serve as a directional single photon source with high light extraction efficiency. The radial intensity distributions of Figure 2c,d along the green dashed lines are shown in Figure 2e,f, respectively. The red vertical lines mark the maximum radial collection angle of the objective with NA = 1.4, which indicates that most of the emission into the glass substrate was collected by the objective we used.

We also calculated the percentage of emission light going to the glass side for the reference QD, coupled QD, and NW end scattering. The result is 0.83 for the reference QD, 0.84 for the coupled QD, and 0.85 for the NW end scattering (see Section 8 of Supporting Information). Based on the numerical simulations and the measured angular emission distributions, we determine that the collection efficiencies of our objective for the reference QD emission, coupled QD emission, and NW end scattering are C_0 = 83%, C_m = 84% and C_{end} = 85%, respectively. It is reasonable to use the same value for these efficiencies as we do in this paper. Based on measured intensity ratio I_m/I_0 = 0.86 ± 0.06, lifetime τ_m = 11.6 ns, and quantum yield of reference QDs $\eta_{rad,0}$ = 25% (measured using a calibrated integrating sphere method),[47] the free space radiative decay rate of the QD A can be obtained as 0.0186 ± 0.0013 ns^{-1} according to eq 3.

Based on the recorded PL time traces, we can also get the ratio of exciton decay rate of channels II and I, i.e. $k_{SP}/k_{rad,m}$.[25] This value can be expressed as follows:

$$\frac{k_{SP}}{k_{rad,m}} = \frac{I_B e^{\beta L_{A-B}} + I_C e^{\beta L_{A-C}}}{I_A \delta} \tag{4}$$

where $I_{B(C)}$ is the measured intensity of the scattered light at the NW terminal B (C), I_A is the measured PL intensity of QD A, $1/\beta$ is the propagation length of SPs, $L_{A-B(C)}$ is the distance between the emission spots A and B (C), δ is the transmittance of the NW ends, which is experimentally obtained as 0.68.[25] Given the probability of the energy from the QD going to the two directions along the NW is equal, we can relate the propagation length with the emission intensity of the NW ends as follows:

$$\beta = \frac{1}{L_{A-C} - L_{A-B}} \ln\left(\frac{I_B}{I_C}\right) \tag{5}$$

The accurate positions of the QD A and the two NW ends are obtained by using a maximum likelihood single molecule localization method,[48,49] and they are labeled with red dots in Figure 1c. The position accuracy of this method is about 10 nm for our experimental setup (see Supporting Information Figure S8). The distances between the emission spots are as follows: L_{A-B} = 1899 nm, L_{A-C} = 3270 nm.

From the time traces shown in Figure 1d, the value of I_B/I_C is centered at about 1.32 within the measured time scale (see Supporting Information Figure S9a). A propagation length of about 4938 nm is obtained by solving eq 5. The relationship of emission counts at B and A is as follows:

$$\frac{I_B}{I_A} = \frac{\delta k_{SP}}{2e^{\beta L_{A-B}} k_{rad,m}} \tag{6}$$

We use the time trace at A to fit that at B and obtain the decay rate ratio of $k_{SP}/k_{rad,m}$ = 0.790 ± 0.003 (see Supporting Information Figure S9b). With both $k_{SP}/k_{rad,m}$ and $k_{rad,m}$ obtained, we get the decay rate of the SP generation channel k_{SP} = 0.0147 ± 0.0010 ns^{-1}.

By subtracting the radiative decay rate and the SP generation rate from the total decay rate obtained through the lifetime measurement ($k_{tot,m} = 1/\tau_m$), we extract that the exciton decay rate to nonradiative damping channel is 0.0529 ± 0.0023 ns^{-1}. The quantum yield of single SP generation for this QD-NW system is η_{SP} = 17.1 ± 1.2%, which means that about 17% of the QD energy is transformed into single SP on the NW.

The distance between the QD and the NW is a critical parameter influencing the decay of excitons. Here we control the QD-NW separation by changing the thickness of the Al_2O_3 film. Figure 3a–c shows the measured PL lifetime, PL intensity enhancement factor, and decay rate ratio $k_{SP}/k_{rad,m}$ for different QD-NW separation distances, respectively. In order to minimize the errors caused by the uncertainty of the QD-NW separation and QD orientation, we measured 20 QD-NW coupled systems for each Al_2O_3 thickness. As the separation distances between the QDs and the NW ends in our experiments are usually larger than half of the coherence length of the SP generated by the excited QD, the SP-interference-induced spatial variation of the PL intensity and lifetime could be ignored (see Section 11 of Supporting Information). The change of the lifetime indicates that the excited QD decays faster with decreasing the QD-NW separation. The PL intensity enhancement factor decreases from around 1 at 35 nm to 0.38 at 3 nm. The ratio of exciton decay rate of channel II to that of channel I shows an exponential decrease as the Al_2O_3 film thickness increases from 3 to 35 nm, which means that the interaction between exciton and plasmon is stronger for smaller separations.

DOI: 10.1021/acs.nanolett.5b03654
Nano Lett. 2015, 15, 8181–8187

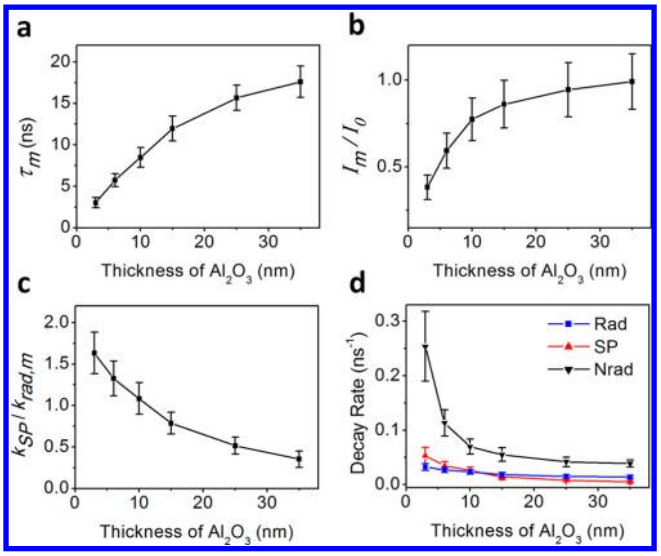

Figure 3. Distance-dependent optical properties of the QD-NW coupling system. PL lifetime (a), PL intensity enhancement factor (b), decay rate ratio $k_{SP}/k_{rad,m}$ (c), and exciton decay rates of the three channels (d) as a function of Al_2O_3 film thickness. The legends "Rad", "SP", and "Nrad" in (d) correspond to the free space radiation channel, SP generation channel, and nonradiative damping channel, respectively. The error bars represent the standard error of the measured data.

Based on the obtained parameters above, we extracted the exciton decay rates of all the three recombination channels as shown in Figure 3d. As the spacer thickness decreases from 35 to 3 nm, the decay rates of all the three channels increase, but the increasing rates are obviously different. The radiative decay rate shows the most moderate increase. When the Al_2O_3 film thickness is 35 nm, the decay rate for SP generation is nearly zero. However, the SP generation rate has a higher increasing rate, and it exceeds the radiative decay rate for Al_2O_3 film thickness smaller than 10 nm. The exciton decay rate of nonradiative damping channel remains almost constant for spacer thickness larger than 15 nm (mainly from the contribution of intrinsic nonradiative decay of the QD). When the thickness is <10 nm, the decay rate of nonradiative damping channel increases quickly and dominates the exciton recombination process.

From the decay rates shown in Figure 3d, we can get the SP quantum yield for different Al_2O_3 thickness as shown in Figure 4a. As the spacer thickness decreases from 35 to 10 nm, the SP quantum yield keeps increasing. Decreasing the spacer thickness from 10 to 3 nm leads to the decrease of SP quantum yield, which is caused by the dramatically increased decay rate of the nonradiative damping channel. The optimum QD-NW distance for efficient exciton−plasmon conversion is about 10 nm, corresponding to a maximum SP quantum yield of 21%. This trend is consistent with the theoretical predictions (see Section 12 of Supporting Information).[50]

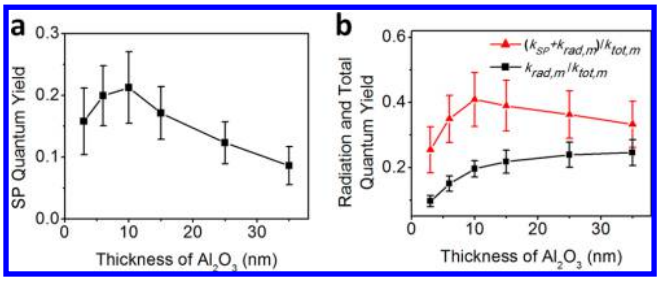

Figure 4. Distance-dependent quantum yields. Experimentally extracted SP quantum yield (a), and radiation and total quantum yield (b) as a function of Al_2O_3 thickness.

Figure 4b shows the radiation quantum yield ($\eta_{rad} = k_{rad,m}/k_{tot,m}$) and the total quantum yield ($\eta_{tot} = (k_{SP} + k_{rad,m})/k_{tot,m}$) for different Al_2O_3 thickness. As can be seen, for Al_2O_3 thickness larger than 15 nm, the radiation quantum yield is little changed and is close to the quantum yield of the reference QDs (25%). As the Al_2O_3 thickness decreases from 15 to 3 nm, the radiation quantum yield decreases fast, which accounts for the change of PL intensity in Figure 3b. For the NW-coupled QD, besides the nonradiative damping, the exciton is recombined by emitting photons and generating SPs on the NW. Thus, the total quantum yield considering both of these two decay channels is the real quantum yield reflecting the energy release of the exciton in the QD.[23,51] For all the Al_2O_3 thicknesses considered here, the total quantum yield is larger than that of the reference QDs (25%). The maximum total quantum yield of 41% is obtained for Al_2O_3 thickness of 10 nm.

These results can be generalized to the coupling systems composed of QEs and other metal nanostructures, where the directly emitted photons from the QEs and the emission of the exciton-generated SPs are difficult to distinguish. For plasmon-enhanced fluorescence in nanoparticle-emitter systems, both the direct radiation and SP-mediated radiation contribute to the intensity of the detected fluorescence. The intensity of the SP-mediated emission is dependent on SP quantum yield and SP scattering efficiency.[23] With the decrease of their separation distance, the direct radiation quantum yield is decreased, and more energy is transferred to the SP-mediated radiation. However, because of the quickly increased nonradiative damping rate, there exists an optimum separation distance for the most efficient generation of SPs.

As an efficient optical nanoantenna, the metal nanostructure can be used to modify the angular emission direction of a single QE, which is usually realized through efficient energy transfer from the emitter to the resonant SP mode of the optical antenna with specific emission angle distribution.[23] The direct far-field emission of the QEs usually does not have preferential direction and thus decreases the directivity of the antenna. Besides, for the nanoamplifiers and nanolasers/spasers based on SPs, the amplification process requires the stimulated emission of SPs generated from the exciton in the gain material.[16] The direct far-field emission does not contribute to the amplification, but enlarges the losses and increases the threshold for the nanodevices. Both of these two examples reveal the different contributions of SP generation channel and the free space radiation channel. Usually, it is necessary to increase the decay rate ratio $k_{SP}/k_{rad,m}$, corresponding to the decrease of separation between the QEs and nanostructures. However, the dramatically increased nonradiative damping rate at smaller separation distances will decrease the SP quantum yield and induce the excessive generation of heat, which needs to be avoided in applications. Thus, we need to balance the three decay channels to optimize the performance of plasmonic devices.

In conclusion, we have experimentally studied the exciton−plasmon coupling process in a system composed of a single QD and a Ag NW. The quantum yield of single SP generation is determined in experiment by quantitatively obtaining the decay

DOI: 10.1021/acs.nanolett.5b03654
Nano Lett. 2015, 15, 8181−8187

rates of all the exciton recombination channels. With the decrease of QD-NW separation, the decay rates of all the three channels increase but with different increasing rates, which leads to an optimum emitter-NW coupling distance of about 10 nm for the highest SP quantum yield and total quantum yield. This work reports the first experimental measurement of SP quantum yield for single QE coupled with plasmonic nanostructure. The results are crucial for optimizing interactions between single emitters and SPs and are important for the design and construction of plasmonic light emitting devices and on-chip quantum plasmonic devices for potential nanophotonic and quantum information applications.

■ ASSOCIATED CONTENT

Supporting Information

The Supporting Information is available free of charge on the ACS Publications website at DOI: 10.1021/acs.nanolett.5b03654.

Details about the numerical calculation of the excitation rate enhancement factor for different Al_2O_3 film thickness, sample preparation and optical measurements, emission model of single reference QD on Al_2O_3-coated glass substrate, the percentage of light going to the glass side for the emission from the reference QD, the coupled QD and the NW end scattering, the coherence length of the SPs generated by the excited QD, theoretical results of the distance-dependent decay rate enhancement factors and SP quantum yield, distance-dependent SP-generation efficiency without considering the non-radiative damping channel, and Figures S1−S12 (PDF)

■ AUTHOR INFORMATION

Corresponding Author

* E-mail: weihong@iphy.ac.cn.

Notes

The authors declare no competing financial interest.

■ ACKNOWLEDGMENTS

We thank Professor Lijun Wu in South China Normal University for the help with measuring the quantum yield of the QDs. We thank Professor Javier Aizpurua, Dr. Mikolaj Kajetan Schmidt, and Deng Pan for the help in simulations. We thank Zhili Jia for the help in measuring the Fourier plane images. We thank the Laboratory of Microfabrication in the Institute of Physics, Chinese Academy of Sciences (CAS) for experimental support. This work was supported by Ministry of Science and Technology of China (grant nos. 2015CB932400 and 2012YQ12006005), National Natural Science Foundation of China (grant nos. 11422436, 11374012, 11227407, 11134013, and 61210017), Prominent Young Scientist Program and Strategic Priority Research Program (B) (grant no. XDB07030100) of CAS, and New-Star of Science and Technology Program of Beijing Municipal Science and Technology Commission.

■ REFERENCES

(1) Chang, D. E.; Sorensen, A. S.; Hemmer, P. R.; Lukin, M. D. *Phys. Rev. Lett.* **2006**, *97*, 053002.
(2) Hakala, T. K.; Toppari, J. J.; Kuzyk, A.; Pettersson, M.; Tikkanen, H.; Kunttu, H.; Törmä, P. *Phys. Rev. Lett.* **2009**, *103*, 053602.
(3) Zhang, J. T.; Tang, Y.; Lee, K.; Ouyang, M. *Nature* **2010**, *466*, 91−95.
(4) Vasa, P.; Wang, W.; Pomraenke, R.; Lammers, M.; Maiuri, M.; Manzoni, C.; Cerullo, G.; Lienau, C. *Nat. Photonics* **2013**, *7*, 128−132.
(5) Barnes, W. L.; Dereux, A.; Ebbesen, T. W. *Nature* **2003**, *424*, 824−830.
(6) Schuller, J. A.; Barnard, E. S.; Cai, W.; Jun, Y. C.; White, J. S.; Brongersma, M. L. *Nat. Mater.* **2010**, *9*, 193−204.
(7) Anger, P.; Bharadwaj, P.; Novotny, L. *Phys. Rev. Lett.* **2006**, *96*, 113002.
(8) Kuhn, S.; Hakanson, U.; Rogobete, L.; Sandoghdar, V. *Phys. Rev. Lett.* **2006**, *97*, 017402.
(9) Chen, X. W.; Agio, M.; Sandoghdar, V. *Phys. Rev. Lett.* **2012**, *108*, 233001.
(10) Lu, D.; Kan, J. J.; Fullerton, E. E.; Liu, Z. W. *Nat. Nanotechnol.* **2014**, *9*, 48−53.
(11) Andrew, P.; Barnes, W. L. *Science* **2004**, *306*, 1002−1005.
(12) Zhou, Z. K.; Li, M.; Yang, Z. J.; Peng, X. N.; Su, X. R.; Zhang, Z. S.; Li, J. B.; Kim, N. C.; Yu, X. F.; Zhou, L.; Hao, Z. H.; Wang, Q. Q. *ACS Nano* **2010**, *4*, 5003−5010.
(13) Kwon, M. K.; Kim, J. Y.; Kim, B. H.; Park, I. K.; Cho, C. Y.; Byeon, C. C.; Park, S. J. *Adv. Mater.* **2008**, *20*, 1253−1257.
(14) Fedutik, Y.; Temnov, V.; Schöps, O.; Woggon, U.; Artemyev, M. *Phys. Rev. Lett.* **2007**, *99*, 136802.
(15) Wei, H.; Ratchford, D.; Li, X. E.; Xu, H. X.; Shih, C. K. *Nano Lett.* **2009**, *9*, 4168−4171.
(16) Berini, P.; De Leon, I. *Nat. Photonics* **2012**, *6*, 16−24.
(17) Lu, Y. J.; Kim, J.; Chen, H. Y.; Wu, C. H.; Dabidian, N.; Sanders, C. E.; Wang, C. Y.; Lu, M. Y.; Li, B. H.; Qiu, X. G.; Chang, W. H.; Chen, L. J.; Shvets, G.; Shih, C. K.; Gwo, S. *Science* **2012**, *337*, 450−453.
(18) Liu, N.; Wei, H.; Li, J.; Wang, Z. X.; Tian, X. R.; Pan, A. L.; Xu, H. X. *Sci. Rep.* **2013**, *3*, 1967.
(19) Munechika, K.; Chen, Y.; Tillack, A. F.; Kulkarni, A. P.; Jen-La Plante, I.; Munro, A. M.; Ginger, D. S. *Nano Lett.* **2011**, *11*, 2725−2730.
(20) Shimizu, K. T.; Woo, W. K.; Fisher, B. R.; Eisler, H. J.; Bawendi, M. G. *Phys. Rev. Lett.* **2002**, *89*, 117401.
(21) Munechika, K.; Chen, Y.; Tillack, A. F.; Kulkarni, A. P.; Plante, I. J.; Munro, A. M.; Ginger, D. S. *Nano Lett.* **2010**, *10*, 2598−2603.
(22) Ratchford, D.; Shafiei, F.; Kim, S.; Gray, S. K.; Li, X. Q. *Nano Lett.* **2011**, *11*, 1049−1054.
(23) Ming, T.; Chen, H. J.; Jiang, R. B.; Li, Q.; Wang, J. F. *J. Phys. Chem. Lett.* **2012**, *3*, 191−202.
(24) Akimov, A. V.; Mukherjee, A.; Yu, C. L.; Chang, D. E.; Zibrov, A. S.; Hemmer, P. R.; Park, H. K.; Lukin, M. D. *Nature* **2007**, *450*, 402−406.
(25) Li, Q.; Wei, H.; Xu, H. X. *Nano Lett.* **2014**, *14*, 3358−3363.
(26) Chang, D. E.; Sørensen, A. S.; Demler, E. A.; Lukin, M. D. *Nat. Phys.* **2007**, *3*, 807−812.
(27) Falk, A. L.; Koppens, F. H. L.; Yu, C. L.; Kang, K.; de Leon Snapp, N.; Akimov, A. V.; Jo, M. H.; Lukin, M. D.; Park, H. K. *Nat. Phys.* **2009**, *5*, 475−479.
(28) Kolesov, R.; Grotz, B.; Balasubramanian, G.; Stohr, R. J.; Nicolet, A. A. L.; Hemmer, P. R.; Jelezko, F.; Wrachtrup, J. *Nat. Phys.* **2009**, *5*, 470−474.
(29) Huck, A.; Kumar, S.; Shakoor, A.; Andersen, U. L. *Phys. Rev. Lett.* **2011**, *106*, 096801.
(30) Frimmer, M.; Chen, Y.; Koenderink, A. F. *Phys. Rev. Lett.* **2011**, *107*, 123602.
(31) Gruber, C.; Trügler, A.; Hohenau, A.; Hohenester, U.; Krenn, J. R. *Nano Lett.* **2013**, *13*, 4257−4262.
(32) Kumar, S.; Kristiansen, N. I.; Huck, A.; Andersen, U. L. *Nano Lett.* **2014**, *14*, 663−669.
(33) Schell, A. W.; Engel, P.; Werra, J. F. M.; Wolff, C.; Busch, K.; Benson, O. *Nano Lett.* **2014**, *14*, 2623−2627.
(34) Ropp, C.; Cummins, Z.; Nah, S.; Fourkas, J. T.; Shapiro, B.; Waks, E. *Nat. Commun.* **2013**, *4*, 1447.
(35) Ropp, C.; Cummins, Z.; Nah, S.; Fourkas, J. T.; Shapiro, B.; Waks, E. *Nat. Commun.* **2015**, *6*, 6558.

DOI: 10.1021/acs.nanolett.5b03654
Nano Lett. 2015, 15, 8181−8187

(36) Dulkeith, E.; Morteani, A. C.; Niedereichholz, T.; Klar, T. A.; Feldmann, J.; Levi, S. A.; van Veggel, F. C. J. M.; Reinhoudt, D. N.; Möller, M.; Gittins, D. I. *Phys. Rev. Lett.* **2002**, *89*, 203002.
(37) Wang, Q.; Stobbe, S.; Lodahl, P. *Phys. Rev. Lett.* **2011**, *107*, 167404.
(38) Johansen, J.; Stobbe, S.; Nikolaev, I. S.; Lund-Hansen, T.; Kristensen, P. T.; Hvam, J. M.; Vos, W. L.; Lodahl, P. *Phys. Rev. B: Condens. Matter Mater. Phys.* **2008**, *77*, 073303.
(39) Stobbe, S.; Johansen, J.; Kristensen, P. T.; Hvam, J. M.; Lodahl, P. *Phys. Rev. B: Condens. Matter Mater. Phys.* **2009**, *80*, 155307.
(40) Chizhik, A. I.; Chizhik, A. M.; Khoptyar, D.; Baar, S.; Meixner, A. J. *Nano Lett.* **2011**, *11*, 1131−1135.
(41) Gersen, H.; Garcia-Parajo, M. F.; Novotny, L.; Veerman, J. A.; Kuipers, L.; van Hulst, N. F. *Phys. Rev. Lett.* **2000**, *85*, 5312−5315.
(42) Curto, A. G.; Taminiau, T. H.; Volpe, G.; Kreuzer, M. P.; Quidant, R.; van Hulst, N. F. *Nat. Commun.* **2013**, *4*, 1750.
(43) Su, L.; Lu, G.; Kenens, B.; Rocha, S.; Fron, E.; Yuan, H.; Chen, C.; Van Dorpe, P.; Roeffaers, M. B.; Mizuno, H.; Hofkens, J.; Hutchison, J. A.; Uji, I. H. *Nat. Commun.* **2015**, *6*, 6287.
(44) Patra, D.; I, G.; Enderlein, J.; Sauer, M. *Appl. Phys. Lett.* **2005**, *87*, 101103.
(45) Li, Q.; Chen, X. J.; Xu, Y.; Lan, S.; Liu, H. Y.; Dai, Q. F.; Wu, L. J. *J. Phys. Chem. C* **2010**, *114*, 13427−13432.
(46) Shegai, T.; Miljkovic, V. D.; Bao, K.; Xu, H.; Nordlander, P.; Johansson, P.; Kall, M. *Nano Lett.* **2011**, *11*, 706−711.
(47) deMello, J. C.; Wittmann, H. F.; Friend, R. H. *Adv. Mater.* **1997**, *9*, 230−232.
(48) Mortensen, K. I.; Churchman, L. S.; Spudich, J. A.; Flyvbjerg, H. *Nat. Methods* **2010**, *7*, 377−381.
(49) Cang, H.; Labno, A.; Lu, C. G.; Yin, X. B.; Liu, M.; Gladden, C.; Liu, Y. M.; Zhang, X. *Nature* **2011**, *469*, 385−388.
(50) Chang, D. E.; Sorensen, A. S.; Hemmer, P. R.; Lukin, M. D. *Phys. Rev. B: Condens. Matter Mater. Phys.* **2007**, *76*, 035420.
(51) Su, H. M.; Zhong, Y. C.; Ming, T.; Wang, J. F.; Wong, K. S. *J. Phys. Chem. C* **2012**, *116*, 9259−9264.

DOI: 10.1021/acs.nanolett.5b03654
Nano Lett. 2015, 15, 8181−8187